

PAPER

The phase diagram of Ti-6Al-4V at high-pressures and high-temperatures

To cite this article: S G MacLeod *et al* 2021 *J. Phys.: Condens. Matter* **33** 154001

View the [article online](#) for updates and enhancements.



IOP | ebooks™

Bringing together innovative digital publishing with leading authors from the global scientific community.

Start exploring the collection—download the first chapter of every title for free.

The phase diagram of Ti-6Al-4V at high-pressures and high-temperatures

S G MacLeod^{1,2,*}, D Errandonea³, G A Cox¹, H Cynn⁴,
D Daisenberger⁵, S E Finnegan², M I McMahon², K A Munro²,
C Popescu⁶ and C V Storm²

¹ AWE, Aldermaston, Reading, RG7 4PR, United Kingdom

² SUPA, School of Physics and Astronomy, and Centre for Science at Extreme Conditions, The University of Edinburgh, Peter Guthrie Tait Road, Edinburgh, EH9 3FD, United Kingdom

³ Departamento de Física Aplicada-ICMUV, Universidad de Valencia, MALTA Consolider Team, Edificio de Investigación, C/Dr. Moliner 50, 46100 Burjassot, Valencia, Spain

⁴ Lawrence Livermore National Laboratory, Livermore, California 94550, United States of America

⁵ Diamond Light Source Ltd., Harwell Science & Innovation Campus, Didcot, Oxfordshire, OX11 0DE, United Kingdom

⁶ CELLS-ALBA Synchrotron Light Facility, Cerdanyola del Vallès 08290, Barcelona, Spain

E-mail: simon.macleod@awe.co.uk

Received 14 December 2020, revised 11 January 2021

Accepted for publication 26 January 2021

Published 18 February 2021



Abstract

We report results from a series of diamond-anvil-cell synchrotron x-ray diffraction and large-volume-press experiments, and calculations, to investigate the phase diagram of commercial polycrystalline high-strength Ti-6Al-4V alloy in pressure–temperature space. Up to ~ 30 GPa and 886 K, Ti-6Al-4V is found to be stable in the hexagonal-close-packed, or α phase. The effect of temperature on the volume expansion and compressibility of α -Ti-6Al-4V is modest. The martensitic $\alpha \rightarrow \omega$ (hexagonal) transition occurs at ~ 30 GPa, with both phases coexisting until at ~ 38 – 40 GPa the transition to the ω phase is completed. Between 300 K and 844 K the $\alpha \rightarrow \omega$ transition appears to be independent of temperature. ω -Ti-6Al-4V is stable to ~ 91 GPa and 844 K, the highest combined pressure and temperature reached in these experiments. Pressure–volume–temperature equations-of-state for the α and ω phases of Ti-6Al-4V are generated and found to be similar to pure Ti. A pronounced hysteresis is observed in the ω -Ti-6Al-4V on decompression, with the hexagonal structure reverting back to the α phase at pressures below ~ 9 GPa at room temperature, and at a higher pressure at elevated temperatures. Based on our data, we estimate the Ti-6Al-4V α - β - ω triple point to occur at ~ 900 K and 30 GPa, in good agreement with our calculations.

Keywords: Ti-6Al-4V, x-ray diffraction, high-pressure, high-temperature, phase transformation, equation-of-state

(Some figures may appear in colour only in the online journal)

1. Introduction

Ti-6Al-4V (wt.%, and hereafter referred to as Ti64) is a two-phase ($\alpha + \beta$) alloy of titanium (Ti) and substitutional aluminium (Al) and vanadium (V). Originally created to stabilise the α -phase character of Ti, Ti64 finds itself utilised across a wide range of industrial and commercial applications,

* Author to whom any correspondence should be addressed.

where superior strength-to-weight ratio, resistance to corrosion and ease of machinability are desirable material properties [1, 2]. Compared with commercial Ti, Ti64 possesses a greater hardness, yield strength and tensile strength [3]. This makes Ti64 particularly attractive to the defence, aerospace and automotive sectors, where there is a constant drive to improve performance by means of greater fuel efficiencies and component fatigue mitigation. Ti64 is also broadly used for

biomechanical applications, including prostheses and implants. Since the mechanical properties of a material are strongly influenced by the underlying microstructure (crystal structures, defects, impurities, grain boundaries), design engineers require materials models that accurately represent these properties. However, without adequate experimental data to constrain and validate these models, uncertainties will inevitably remain. Surprisingly, the crystal structure of Ti64 has rarely been studied under extreme pressure and temperature conditions. This scarcity of data renders the development of a truly predictive Ti64 model challenging. Therefore, there is a clear requirement for more experimentation to address this data deficiency.

At ambient conditions, Ti64 crystallises predominantly in the hexagonal-close-packed (hcp) structure, or α phase (space group $P6_3/mmc$). Around the α phase grain boundaries there exists a smaller fraction by volume of body-centred-cubic (bcc), or β phase (space group $Im3m$) Ti64. The alloying of substitutional elements Al and V, and the presence of interstitial impurities (mostly oxygen, carbon and iron) increases the strength of near- α (hereafter referred to as just α) Ti64 relative to pure Ti [1, 2].

At ambient pressure, Ti64 transforms from α to the mixed ($\alpha + \beta$) phase at ~ 1070 K and then to the more ductile β phase at ~ 1280 K [2]. Melting occurs at 1943 K [4]. Pure Ti, which also crystallises in the α phase at ambient conditions, transforms to β -Ti at 1155 K and melts at ~ 1940 K.

At room temperature (RT), and under static compression in combined diamond-anvil-cell (DAC) and x-ray diffraction (XRD) studies, commercially pure α -Ti64 is stable up to at least 26 GPa [5–8]. The bulk modulus (K_0) and pressure derivative (K_0') for α -Ti64 embedded in neon, a quasi-hydrostatic pressure-transmitting-medium (PTM), were found to be $K_0 = 101(3)$ GPa, and $K_0' = 4.1(3)$ [6, 7], respectively. With no PTM present, thus resulting in the α -Ti64 sample experiencing a strong uniaxial stress along the direction of load, $K_0 = 154(11)$ GPa and $K_0' = 5(1)$ [8], suggesting a link between compressibility and the hydrostaticity of the pressure environment [8]. α -Ti64 martensitically transforms to the more brittle hexagonal ω -phase (space group $P6/mmm$) at 26–33 GPa [5–7]. The $\alpha \rightarrow \omega$ transition is sluggish and completely transforms by ~ 45 GPa [6]. The corresponding volume reduction at $\alpha \rightarrow \omega$ is $-\Delta V/V \sim 1\%–2\%$ [5–7]. The Ti64 samples studied were of the commercial variety, and hence low purity [5–8]. On decompression from 70 GPa back to 0.8 GPa, α -Ti64 was recovered from ω -Ti64 [6]. This $\alpha \rightarrow \omega$ transition sequence is common to group IVB metals Ti, zirconium (Zr) and hafnium (Hf) [9, 10]. In Ti, the $\alpha \rightarrow \omega$ transition occurs at 3–14.6 GPa [11–20] and appears to be sensitive to impurity content and the presence of non-hydrostatic stress conditions [16]. For α -Ti, $K_0 = 102–117$ GPa, and for ω -Ti, $K_0 = 107–142$ GPa [13–20], depending on the PTM. Just like Ti64, Ti has a higher compressibility in a more hydrostatic environment. Unlike Ti64, the $\alpha \rightarrow \omega$ transition is strongly dependent on the PTM, with the transition taking place at higher pressures in more hydrostatic environments [16, 19]. The $\alpha \leftrightarrow \omega$ transformation exhibits a considerable hysteresis in a hydrostatic environment, with ω -Ti remaining after decompression [12,

13, 19], though in the presence of shear stress, ω -Ti reverts to α -Ti after pressure release [16].

Under further compression at RT, ω -Ti64 transforms sluggishly to a bcc-type phase, which is isomorphic to high-temperature (HT) β -Ti64 and has been proposed (but not probed yet) to be the same phase. To distinguish the two phases, we will name the RT high-pressure phase as β' -Ti64. This transition occurs at ~ 94 GPa, and completes at 127–128 GPa, with a reduction in volume at $\omega \rightarrow \beta'$ of $-\Delta V/V < 2\%$ [6]. The transition to β' -Ti64 is characterised by the gradual reduction in intensity of the (001), (101), (111), (002) and (112) ω -Ti64 peaks in the XRD patterns until only β' phase peaks remain. At RT, β' -Ti64 is stable to at least 220 GPa [6, 7]. Density functional theory calculations confirm the $\alpha \rightarrow \omega \rightarrow \beta'$ transformation pathway to be the most likely sequence for Ti64 at RT, but the transition pressures are only consistent with experiment if calculations are performed on the assumption that significant local atomic ordering occurs during compression [6].

Ti does not undergo the $\alpha \rightarrow \omega \rightarrow \beta'$ RT pathway followed by Ti64 and the other Group IVB metals, Zr and Hf [9, 10]. ω -Ti transforms to an orthorhombic (space group $Cmcm$) γ phase (distorted hcp) at 115–128 GPa, and then to an orthorhombic (space group $Cmcm$) δ phase (distorted bcc) at 135–145 GPa [13, 14, 17]. The δ phase has been reported to transform back to the β' phase at 243 GPa, which is stable to at least 290 GPa [22]. In one study [15], a mixed phase ω -Ti and β' -Ti was reported between 40 GPa and 80 GPa. After laser-heating at 78–80 GPa, an orthorhombic η -Ti (space group $Fm\bar{3}m$) structure emerged that reverted back to pure β' -Ti below 40 GPa after quenching to RT, and then finally transformed to ω -Ti below 30 GPa [15]. The thermal properties of Ti have been studied up to 200 GPa and 3500 K [15, 19–23]. Thermal equations-of-state (EoSs) have been generated for α -Ti, ω -Ti [21] and β -Ti [20], and the α - β - ω triple point was estimated to lie at ~ 8.0 GPa and > 900 K [19, 20]. The hysteresis in the $\alpha \leftrightarrow \omega$ transformation at HT is reduced compared with RT, with partial ω -Ti reportedly still present at ~ 2 GPa and 737 K [20]. After quenching β -Ti from 3000 K, the δ -Ti phase subsequently reappeared under compression, suggesting the δ phase is not metastable [20].

Shock experiments have yet to verify the $\alpha \rightarrow \omega$ transition in Ti64 [24–30] though this may be due to the difficulty in detecting the small volume change across the phase boundary [24, 26]. Sollier *et al* [29] shock compressed Ti64 up to 52 GPa and observed a dip in the release isentrope at ~ 27 GPa. This feature may correspond to the α - β - ω triple point at 30 GPa and 850 K, predicted using the particle swarm optimization (PSO) technique [31, 32]. α -Ti has been observed to transform to ω -Ti at 10.1–14.3 GPa under shock compression [34–37]. The presence of impurities in Ti, notably interstitial oxygen, strongly influences the shock $\alpha \rightarrow \omega$ transition pressure: for high purity Ti (oxygen content 360 ppm), the transition pressure was 10.4 GPa, whereas for low purity Ti (oxygen content 3700 ppm), no transition was observed up to 35 GPa [36].

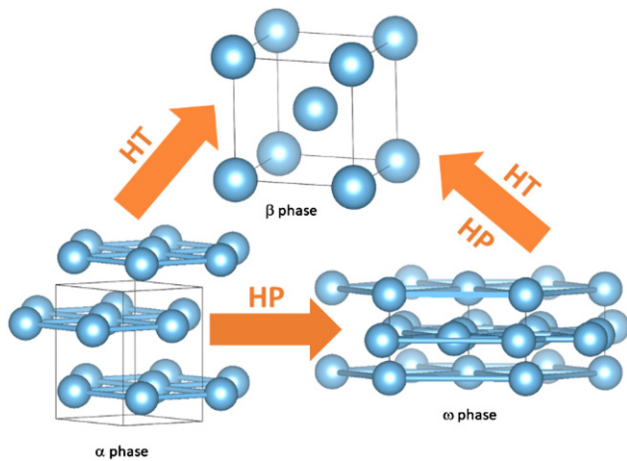


Figure 1. The transformation pathway of Ti-6Al-4V at high-pressure and HT.

Very few calculations of the Ti64 pressure–temperature (P – T) phase diagram have been attempted (see section 3.2 for a discussion of the PSO method), primarily due to a lack of experimental data to constrain the models [32, 34]. On the other hand, considerable effort has been expended on the Ti phase diagram and on developing a better understanding of the $\alpha \rightarrow \omega$ transition mechanism [38–50]. Cold curve calculations agree with the sequence $\alpha \rightarrow \omega \rightarrow \gamma$ [40, 42, 43, 45, 46], but disagreements exist concerning the subsequent pathway as either $\gamma \rightarrow \beta'$ [40, 43] or $\gamma \rightarrow \delta \rightarrow \beta'$ [42, 46], largely based on considerations of phase stability under hydrostatic conditions. At RT, Joshi *et al* predict $\omega \rightarrow \beta'$ [38], and in a joint experimental and theoretical study, $\omega \rightarrow \beta'$ has also been proposed as the structural pathway [15].

The energetics and kinetics driving the martensitic $\alpha \rightarrow \omega$ transformation have been considered and intermediate metastable states have been contemplated [47–51]. The so-called TAO-1 pathway was found to have the lowest activation enthalpy for the $\alpha \rightarrow \omega$ transformation [47–49]. In addition, interstitial and substitutional impurities have been calculated to suppress the transition by increasing the energy barrier of the TAO-1 transformation [49].

Interstitial oxygen has more significance than nitrogen and carbon in suppressing the $\alpha \rightarrow \omega$ transition in pure Ti [49], as borne out by experiment [36]. Even a low density body-centred orthorhombic (bco) metastable structure might be stabilised through the manipulation of impurities [51].

In summary, given its widespread utility across industry and commerce, it is surprising how seldom Ti64 has been studied experimentally and theoretically at extreme pressures and temperatures [5–8, 24–30, 32–34]. By contrast, the available literature on Ti is quite extensive [11–23, 33–51]. Here we report results from a series of high-pressure high-temperature (HP–HT) experiments to investigate the structural pathway of Ti64 (see figure 1) and benchmark these results against published Ti data.

2. Experimental details

Powdered samples of commercial polycrystalline Ti64, possessing an impurity level of 0.123 wt.%, were procured from Goodfellow. The purity level of the Ti64 was equivalent to an oxygen content of approximately 3700 ppm in pure Ti. Produced by Goodfellow using a patented approach known as plasma atomization, these samples can be characterised as low purity [52]. The Ti64 samples used in this study were sourced from the same batch used in a previous RT study performed by us [6, 7].

2.1. DAC experiments

Samples of Ti64 powder were loaded into eight gas membrane-driven piston and cylinder DACs, together with one or more of the following: potassium chloride (KCl), sodium chloride (NaCl), magnesium oxide (MgO), and copper (Cu), as the PTM and/or pressure marker. The thermal EoSs for these materials are known and can be used to determine pressure values from XRD patterns at HP–HT [53–56]. Spark-eroded rhenium (Re) discs were used as the gasket material (pressure chamber). We chose a variety of pressure media to reduce the risk of potential chemical reactions at HT. Diamond culet diameters ranged from 200 μm to 300 μm and the pressure chamber diameters < 100 μm .

For HP–HT measurements, our DACs were placed inside a dedicated water-cooled vacuum vessel and heated with a coiled Watlow resistive heater (rated at 4.65 W cm^{-2}), wrapped around the outside of the DACs [57]. To prevent diamond oxidation and convective heating inside the vessel, vacuum pressures < 10^{-5} mbar level were maintained using a rotary-backed turbo pump. Water cooling the vacuum vessel limits the effects of thermal transfer from the heater and improves the positional stability of the sample relative to the x-ray microfocus. Temperatures were measured using a K-type thermocouple attached to the DAC piston, close to the diamond anvils. The accuracy of temperature measurements is better than 0.4%. In our experience, the practical upper limit in temperature that samples can be heated to using this apparatus is ~ 900 K (for example, [58–60]). To ensure the conditions inside the DACs were as close to thermal equilibrium as practicable, the Ti64 samples were initially compressed to a low pressure (< 5 GPa) in the α phase and then heated up slowly at a rate of ~ 100 K hr^{-1} to a target temperature. Isotherms were then collected in small pressure steps (< 1 GPa) at the target temperature.

Data were mostly collected at beamlines I15 at diamond light source (DLS) and BL04-MSPD at the ALBA synchrotron [61]. The monochromatic x-ray wavelength was 0.4133 Å (30 keV) at I15 and 0.4246 Å (29.2 keV) at BL04. The FWHM of the x-ray beam microfocus at I15 and BL04 was ≤ 20 μm . The detector used at I15 was a Mar345 image plate detector and at BL04 a Rayonix CCD. Additional data were collected at the high pressure collaborative access team beamline 16-

BMD, at the advanced photon source (APS). The x-ray wavelength was 0.4133 Å (30 keV) and the detector used was a Mar345 CCD.

In total, eight isotherms were collected from initial temperatures of 298, 418, 517, 586, 642, 713, 844 and 886 K. All of the 2D angle-dispersive XRD (ADXRD) patterns were integrated azimuthally using Fit2D [62] or DIOPTAS [63]. The resulting 1D profiles were analysed by applying a Le Bail refinement using GSAS [64] or by performing a least-squares fitting of the d spacings of individual peaks using the JADE 9 [65] and unitcell [66] programs. Only XRD patterns containing reflections from both the sample and the pressure marker were analysed.

2.2. Bridgman-type cell experiments

To complement the DAC experiments, we performed lab-based experiments using a Bridgman-type belt apparatus. This device consists of a 150 ton oil-press containing steel-belted Bridgman-type opposed tungsten-carbide anvils. The sample is contained in a pyrophyllite gasket with hexagonal boron nitride acting as the PTM. The sample pressure is determined by calibrating the load applied to the anvils against high-pressure resistivity transitions in calibrant materials, see for example [67, 68]. Though the calibrant data is limited in range, for pressures above 10.5 GPa a linear extrapolation can be applied to the calibration [68]. The heating element consists of a graphite block connected to a 100 A power supply. Temperatures in the pressure chamber are measured using a shielded K-type thermocouple with an accuracy <3% [69].

This device is capable of pressurising samples to 13 GPa at temperatures up to 1600 K [69, 70]. Resistivity measurements are made across samples using the four probe method. Discontinuities in the measured electrical resistance are indicative of a material phase change. For this study, three experiments were performed on samples of Ti64 sourced from the same batch used in the DAC experiments.

3. Results and discussion

3.1. HP RT DAC XRD experiment

We performed one compression run at 298 K from 2.95(6) GPa to 66(1) GPa. The Ti64 sample was embedded in KCl, which acted as both the PTM and pressure marker. A Sanchez-technologies pressure control system (maximum output 1000 bar) was used to regulate the DAC membrane-pressure. A time interval of 2–3 min between membrane-pressure increase and data collection ensured the sample pressure was always close to equilibrium. At 6.4 GPa, the pressure gradient across the pressure chamber (gasket hole diameter <100 μm) was 0.3 GPa. The results at RT are in excellent agreement with previous studies [5–7]. Thus, for the sake of brevity (and to avoid redundancies) we do not show a selection of RT XRD patterns. In our experiments, the emergence of the dominant ω -Ti64 (110/101) peaks at 30(1) GPa signified the onset of the $\alpha \rightarrow \omega$ transformation. This sluggish transformation to the ω phase was completed at 40.7(8) GPa. The measured volume reduction $-\Delta V/V$, from α - to ω - was <2%.

The KCl B2 Vinet EoS parameters used to generate pressure values at 298 K, as a function of volume, were: $V_0 = 54.5 \text{ \AA}^3$, $K_0 = 18.3(3) \text{ GPa}$ and $K'_0 = 5.60(3)$ [53], where V_0 is the ambient cell volume.

The c/a axial ratio for α -Ti64 was found to be almost invariant under pressure, fluctuating between 1.595 and 1.602 between 2.95(6) GPa and 33.1(6) GPa, again in good agreement with previous measurements [6, 7]. These values are smaller than the ideal value of 1.633 for the α phase. For ω -Ti64, c/a has a slightly positive slope, rising from 0.612 (the ideal value) to 0.617 between 34.8 GPa and 65.5 GPa. The calculated c/a ratio for ω -Ti64 at 0 K, due to local ordering of Al and V, rises from 0.616 at 20 GPa to 0.618 at 60 GPa, and then drops to 0.615 at 100 GPa [6].

The sample was slowly decompressed from 66(1) GPa, to reveal a strong hysteresis, with the ω phase stable to $\sim 9.1(1)$ GPa. A sudden jump in pressure to 3.2(1) GPa resulted in the Ti64 completely reverting back into the α phase. But unlike ω -Ti under quasihydrostatic conditions [11, 12], ω -Ti64 is not metastable at ambient pressure after pressure release [6]. Errandonea *et al* [16] recovered α -Ti from ω -Ti at RT, after decompressing a Ti sample embedded in NaCl, a similar PTM to KCl. But α -Ti was not detected after pressure release for ω -Ti embedded in the more hydrostatic PTMs argon and 4:1 methanol-ethanol [16] and helium [19]. In our earlier study of Ti64, we decompressed ω -Ti64 from 70 GPa to 0.8 GPa in a methanol-ethanol PTM and recovered α -Ti64 [6].

A discussion of the RT EoS will be conducted in section 3.3 in combination with the analysis of the HP-HT results. Here we would like just to mention that a 3rd order Birch-Murnaghan (BM3) EoS [71] fit to the α -Ti64 data generated the EoS parameters, $V_0 = 17.25(4) \text{ \AA}^3$, $K_0 = 110(2) \text{ GPa}$ and $K'_0 = 3.8(2)$. For ω -Ti64, a BM3 fit generated $V_0 = 16.8(2) \text{ \AA}^3$, $K_0 = 115(8) \text{ GPa}$ and $K'_0 = 4.6(8)$. A Vinet [72] fit to the data returned similar values. These EoS results are consistent with published data for Ti64 [5–7] and pure Ti [13–17, 20].

3.1.1. HP-HT DAC XRD experiments. Seven HP-HT isotherms were collected at 418(2), 517(2), 586(2), 642(3), 713(1), 844(5) and 886(2) K. All DACs were precompressed to ~ 5 GPa in the α phase at RT and then heated to a target temperature and compressed into the ω phase. To control the gas-membrane pressure to our DACs, we used a Sanchez-technologies control system at ALBA and a Druck PACE 5000 (maximum output 210 bar) at DLS and the APS. With the exception of the isotherms collected at 418 K and 642 K, all samples were compressed until diamond or gasket failure.

The first set of HP-HT experiments were performed at DLS (isotherms at 517, 642 and 886 K). All DACs were loaded with α -Ti64, NaCl as the PTM, and Cu as the pressure marker. The Cu P - V - T EoS used to generate pressure values comprised a BM3 for RT and a Mie-Grüneisen-Debye (MGD) term for the thermal effects [56].

In figure 2, a waterfall plot of integrated ADXRD patterns, collected at 642 K, shows the $\alpha \rightarrow \omega$ transition and demonstrates the sluggish nature of the transition. The XRD patterns

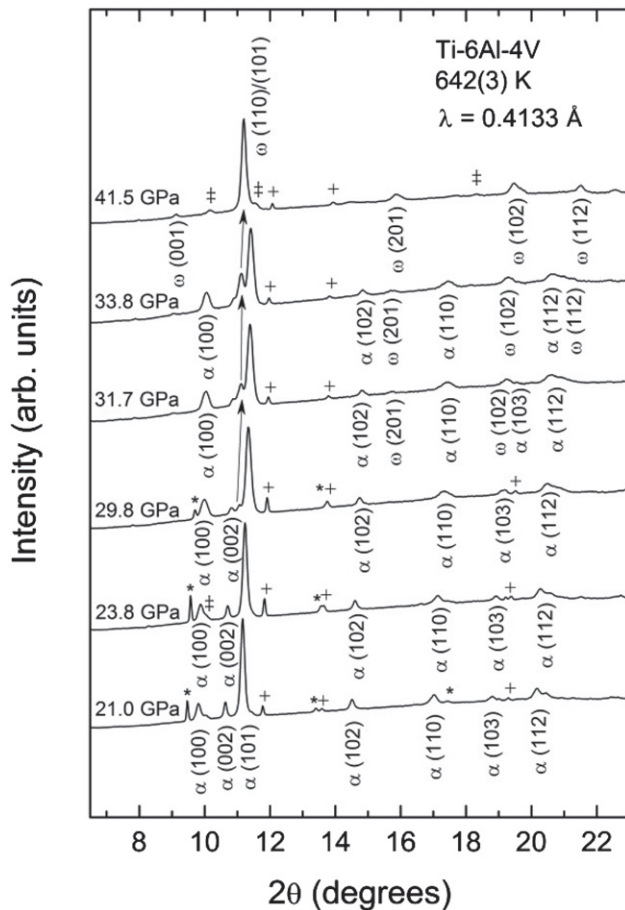


Figure 2. A waterfall plot of integrated ADXRD patterns showing the $\alpha \rightarrow \omega$ transformation in Ti-6Al-4V with increasing pressure at 642(3) K. The vertical arrow at 29.8 GPa points to the emergent ω (101)/(110) peaks. * represents reflections from B1 NaCl, + reflections from Cu, and ‡ reflections from Re. Less prominent peaks are not labelled.

are affected by preferred orientation due to limitations in the experimental apparatus. However, this does not affect phase identification. The dominant ω phase (101)/(110) peaks appear at $\sim 29(1)$ GPa (the peak positions are indicated by the vertical arrow at 29.8 GPa) and grow in intensity with increasing pressure, while simultaneously the α phase peaks gradually diminish in intensity, until at ~ 40 GPa the transformation is complete. The volume change from α to ω phase, $-\Delta V/V \sim 1.7\%$. The pressure range of $\alpha + \omega$ phase coexistence of ~ 10 GPa at 642 K matches that observed at RT. This DAC was compressed to 65 GPa at 642 K into the ω phase. On decompression back to 32 GPa and 642 K, Ti64 was still stable in the ω phase. An unexpected drop in pressure to 8 GPa resulted in the complete transformation back into α -Ti64. Piston and cylinder DACs often seize, then jump, during decompression at HT, leading to irregular intervals in sample pressure. This DAC was cooled down to 517 K and recompressed back into the ω phase at 30(1) GPa, with a phase coexistence extending over a range of ~ 9.5 GPa. Diamond failure in the ω phase occurred at ~ 45 GPa. For both isotherms the volume reduction from α -Ti64 to ω -Ti64, $-\Delta V/V < 2\%$. Pure

Ti remains in the ω phase if released back to ambient pressure at 444 K, but at 737 K there is a partial recovery of the α phase after decompression [19]. An isotherm collected at 886 K, the highest temperature reached in our DAC experiments, terminated early at ~ 23 GPa in the α phase due to gasket failure.

A second series of HP-HT DAC experiments were performed at ALBA (isotherms at 418, 586 and 713 K). Samples of α -Ti64 were embedded in KCl, which acted as both the PTM and pressure marker. Pressure values were generated using a B2 KCl EoS consisting of a Vinet RT term and an MGD thermal term [53]. The transition pressures for $\alpha \rightarrow \omega$ were: 30.0(3) GPa at 418 K, with a phase coexistence of ~ 8.3 GPa; 31(1) at 586 K, with a coexistence of ~ 8.5 GPa; and $\sim 31(1)$ GPa at 713 K, with a coexistence of ~ 8 GPa. Again, $-\Delta V/V$ from α -Ti64 to ω -Ti64, was $< 2\%$. The sample at 418 K was compressed to 49.4 GPa in the ω phase and then released back to 21.9 GPa, still in the ω phase. Upon cooling to RT and 24.7 GPa, the sample still retained the ω phase. Seizure of the cell prevented any further measurements. The 586 K and 713 K isotherms were terminated at 44 GPa and 67 GPa due to gasket failure. At 713 K, the pressure gradient across the chamber (gasket hole $< 100 \mu\text{m}$) at 22.7 GPa was 1.4 GPa. At 713 K and 48.6 GPa, the pressure gradient was 1.7 GPa. To avoid contamination of the XRD patterns from the gasket, we collected all of our patterns as close to the centre of the pressure chamber as possible and to reduce the effects of the pressure gradient.

An additional isotherm at 844 K was collected at the APS, this time using MgO as the PTM and pressure marker. The onset of the $\alpha \rightarrow \omega$ transition was observed at 29(2) GPa, with a coexistence region of ~ 8 GPa before completion of the transformation to the ω phase. ω -Ti64 was stable up to the highest pressure achieved, 93(1) GPa. Due to peak overlap and Re contamination it was not possible to measure the volume reduction across the α - ω phase boundary. In figure 3 we show an integrated ADXRD pattern of ω -Ti64 at 91(1) GPa and 848 K. The unit-cell parameters for the ω -Ti64 pattern in figure 3 are $a = 3.9617(27) \text{ \AA}$ and $c = 2.4666(12) \text{ \AA}$.

Pressure values were generated using a combined BM3 and modified MGD thermal EoS for MgO [55]. Unfortunately we did not detect a measurable lowering in intensity of the (001), (101), (111), (002) and (112) ω peaks to indicate the onset of the predicted $\omega \rightarrow \beta'$ transformation. However, based on our analysis, the simulated intensity of the (101) peak relative to the (110) begins to decrease at ~ 85 GPa. In figure 3, as the (101) and (110) start to separate, the (101) peak becomes a shoulder and introduces an asymmetry into the overall profile, which is consistent with the behaviour we observed at ~ 88 GPa in our previous RT experiment as ω -Ti64 transformed to β' -Ti64 [6]. In the current experiment, the run terminated at ~ 93 GPa due to diamond failure.

For all HP-HT experiments, the c/a axial ratio trend for α -Ti64 is effectively invariant under pressure, indicating isotropic compression, see figure 4. In the plot, the c/a ratio for the α phase at RT, 586 and 844 K averages as 1.597(8). The c/a ratio for ω -Ti64, on the other hand, appears to increase monotonically from the ideal ratio $\sim 0.613(1)$ at ~ 30 GPa to

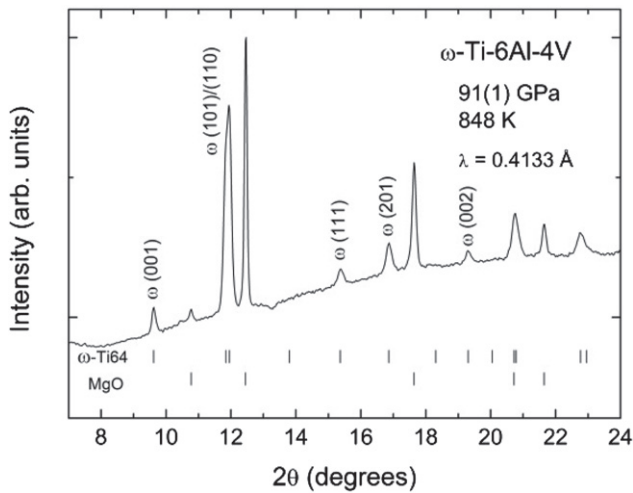


Figure 3. An integrated ADXRD pattern showing ω -Ti-6Al-4V at 91(1) GPa and 848 K. MgO was used as the pressure marker and pressure transmitting medium. The prominent ω phase peaks are indexed. The tick marks beneath the profile indicate the ω phase and MgO diffraction peaks. Note the splitting of the dominant ω (101)/(110) peaks at $\sim 12^\circ$.

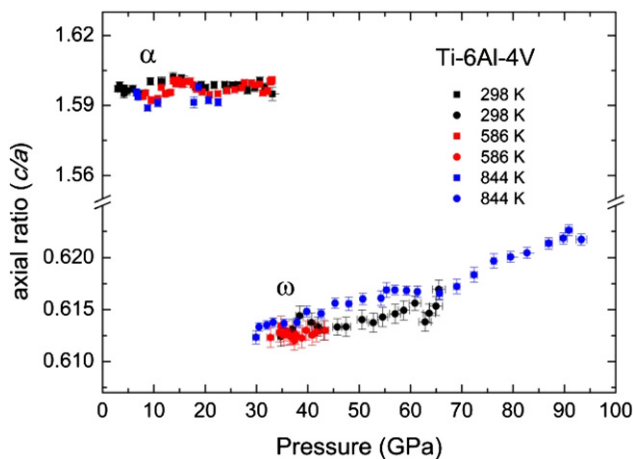


Figure 4. A plot of axial ratios for α -Ti-6Al-4V and ω -Ti-6Al-4V, as a function of pressure, at 298, 586 and 844 K. Square datapoints represent α -Ti-6Al-4V and circular datapoints represent ω -Ti-6Al-4V.

$\sim 0.622(1)$ at ~ 91 GPa. The slope also seems to be independent of temperature. This behaviour is not universally observed in Ti HP experiments. A constant c/a ratio ~ 0.6125 for ω -Ti was reported up to 8.1 GPa in a large press at RT [20], whereas in DAC experiments at RT, the c/a ratio for ω -Ti rises in a similar fashion to our ω -Ti64 data, but starting from a much lower $\alpha \rightarrow \omega$ transition pressure [17–19].

3.1.2. Bridgman-type cell experiment. Three isobaric experimental runs were performed using the Bridgman-type cell apparatus and resistivity measurements were made using the four-probe method. In figure 5, the change in electrical resistivity as a function of temperature is shown for Ti64 at 4.0(2), 8.0(2) and 12.0(2) GPa. The sudden decrease in the measured resistivity is indicative of a material transformation. This

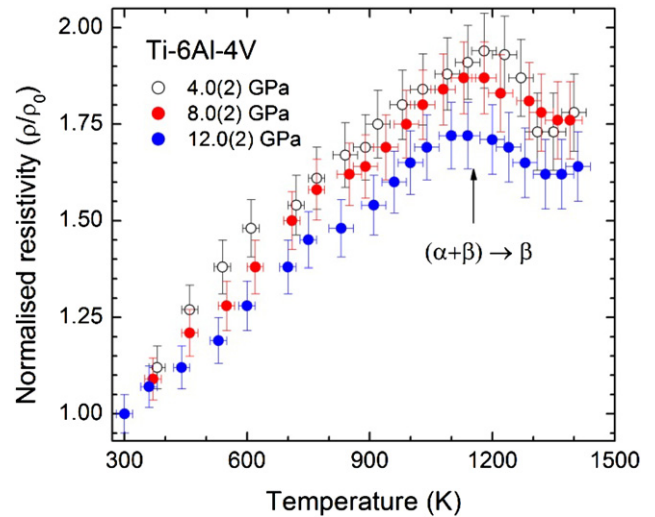


Figure 5. A plot showing the measured changes in resistivity of Ti-6Al-4V at 4.0(2), 8.0(2) and 12.0(2) GPa, as a function of temperature. ρ_0 corresponds to the ambient conditions resistivity measurement.

change of resistivity on its own does not provide evidence for the $\alpha \rightarrow \beta$ phase transition in Ti64. However, since Ti64 is a near- α two-phase $\alpha + \beta$ alloy at ambient conditions, and is known to transform at ambient pressure to the $\alpha + \beta$ phase at ~ 1070 K [2], the modest change observed in the slope for $((d\rho/\rho_0)/dT)$ at 1230(30) K at 4.0(2) GPa; 1180(30) K at 8.0(2) GPa; and 1140(30) K at 12.0(2) GPa, is likely caused by the growth of β phase grains. Similar experiments performed on hcp Ti, Zr and Gd at HP–HT in a large press found the measured resistivity increased with increasing temperature and decreased with increasing pressure [73]. The slight change in slope for isobaric data collected at temperatures up to ~ 900 K suggested the $\alpha \rightarrow \omega$ transformation in Ti occurred above 2 GPa at HT [73]. The α -Ti64 plots in figure 5 appear to confirm the relationship between resistivity and temperature, and resistivity and pressure.

3.2. HP–HT phase diagram

The Ti64 pressure–temperature (P – T) phase diagram is shown in figure 6. The DAC data and Bridgman-type cell data from this study are shown alongside RT data collected by us in an earlier study [6]. Based on the DAC data, the α – ω phase boundary appears to be almost vertical in P – T space. The slope of the α – ω phase boundary, $dT/dP \sim 550$ K GPa $^{-1}$. The slope of the α – ω phase boundary for pure Ti was reported by Zhang *et al* to be 345 K GPa $^{-1}$ [22]. The Bridgman-type cell data lie on a slope given by $dT/dP \sim -11.3$ K GPa $^{-1}$. The black dashed line denotes the proposed solid–solid boundaries for the α – ω and $(\alpha + \omega)$ – β phases. Extrapolating the black dashed line from the Bridgman cell data towards the proposed α – ω phase boundary suggests the α – β – ω triple point occurs at ~ 30 GPa and ~ 910 K.

The black dot-dot-dash line indicates the upper pressure bound of the mixed-phase $(\alpha + \omega)$ region, beyond which, ω -Ti64 is stable. The width of this region of coexistence does not change significantly with increasing temperature. It

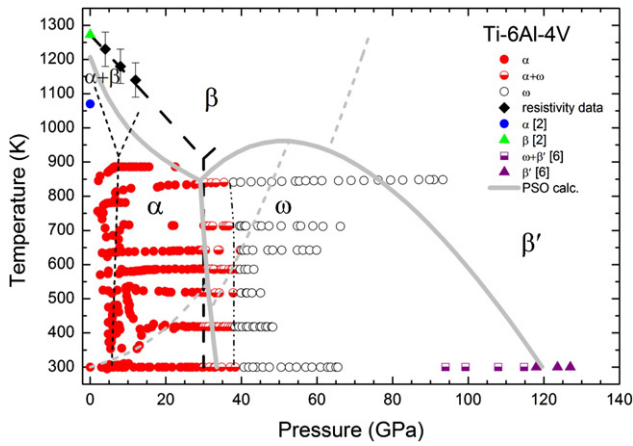


Figure 6. The P - T phase diagram of Ti-6Al-4V. Experimental data from this study are represented by: red circles, α -Ti64; half-red half-white circles, mixed phase ($\alpha + \omega$)-Ti64; white circles, ω -Ti64; black diamonds, phase changes measured using the Bridgman-type cell. Experimental data from previous work are represented by: blue circle, α -Ti64 [2]; green triangle, β -Ti64 [2]; half-purple half-white squares mixed phase ($\omega + \beta'$)-Ti64 [6]; purple triangles β' -Ti64 [6]. The black dashed lines act as a visual guide for the proposed α - ω and ($\alpha + \beta$)- β phase boundaries based on our data. The black dashed-dot line indicates the complete transition to ω -Ti64 from the mixed phase ($\alpha + \omega$)-Ti64. The solid grey lines represent the solid-solid phase boundaries calculated using the PSO technique; and the dashed grey lines the Hugoniot, also calculated using the PSO. The black short dashed lines represent the solid-solid phase boundaries of pure Ti measured by Zhang *et al* [21].

reduces from ~ 10 GPa at RT to ~ 8 GPa at 844 K, which suggests the kinetic barrier in the transformation to the preferred ω phase is weakly dependent on temperature and hydrostaticity. Once transformed, ω -Ti64 extends to at least ~ 93 GPa and 850 K. In this P - T diagram there are regions where we have observed the coexistence of the α and ω phases. Phase coexistence could be affected by Al redistribution between the α and ω phase. However, the exact Al content in each phase cannot be accurately determined from our experiments. Since the quantity of Al in Ti64 is known to vary between 5.7 and 6.5%, we expect the Al redistribution to not significantly affect our results.

The solid and dashed grey lines in figure 6 represent the solid-solid phase boundaries and the Hugoniot, calculated using the PSO technique [31, 32]. The PSO is a stochastic analysis technique that fits statistical mechanics-based condensed matter models to wide ranging datasets. For solid phases, an EoS can be generated by combining contributions to the Helmholtz free energy from a cold curve calculation, thermal ion term, and thermal electron term. In this study, the cold curve was calculated using the augmented stabilised jellium EoS (ASJEOS) [74], which requires only three inputs: ρ_0 , K_0 and K'_0 , where ρ_0 is the density. The thermal ion term combines a mean field model [75] with an Einstein density of states model, where the Einstein temperature is given by

$$\theta_E = \frac{h}{2\pi k} \epsilon^{1/3} \rho^{5/6} (2(2 - \lambda) E'_C + 3\rho E''_C)^{1/2}, \quad (1)$$

Table 1. Multiphase EoS parameters for Ti-6Al-4V, generated using the PSO technique. Parameters λ and ϵ represent model choices for the solid phase and do not change during the PSO calculations.

Parameter	α -Ti-6Al-4V	β -Ti-6Al-4V	ω -Ti-6Al-4V
ρ_0 (g/cc)	4.4615	4.5075	4.6578
K_0 (GPa)	119.78	131.01	156.58
K'_0	3.2518	2.7469	2.7799
λ	-1	-1	-1
ϵ	0.70711	0.76980	0.70711
Boundary	Ambient	α - β	α - ω
P_1 (GPa)		0.0001	33
T_1 (K)		1207	300
P_2 (GPa)		29	29
T_2 (K)		846	846

where the derivatives of the cold curve energy E_C , are with respect to density; ϵ is a constant dependent on the lattice structure; λ takes the value -1 , 0 , or $+1$, which gives rise to the Slater, Dugdale-MacDonald, or Vaschenko-Zuberov Grüneisen functions when calculated using $\Gamma = -\partial \ln \theta_E / \partial \ln V$, where Γ is the Grüneisen parameter and V is the volume. The Thomas-Fermi model represents the electronic term. The EoS along a phase boundary is calculated using the method of mixtures [76]. To predict a phase boundary, the Gibbs free energies are forced to be equal at two specified starting P - T points, which are constraints described by experimental data. No constraints exist for subsequent calculated points in P - T space.

Since the PSO method does not incorporate metastable or two-phase regions in calculations, phase boundaries in P - T space are generated as single points only [32]. As such, the PSO α - β phase boundary in figure 6 is a little misleading. The ($\alpha + \beta$) mixed phase region is currently treated as β -Ti64 using the PSO technique, hence the apparent disagreement between the predicted α - β phase boundary and our proposed ($\alpha + \beta$)- β phase boundary. Nonetheless, the α - β - ω triple point, predicted by PSO to occur at 30 GPa and 850 K [32], is in reasonable agreement with our inferred triple point. The parameters obtained from the PSO fitting process are presented in table 1. In figure 6, the calculated value for the RT ω - β' phase boundary appears to be a little high at ~ 120 GPa, compared with our previous measurement for $\omega \rightarrow \beta'$ of ~ 95 -120 GPa [6].

At 848 K, there is a suggestion in our current dataset that the $\omega \rightarrow \beta'$ transition may be occurring at ~ 85 GPa, but PSO predicts the transition below 80 GPa. This could be related to the use of the Einstein model, which neglects anharmonicity, and which has been found to be relevant for the bcc structure (β -phase) in metals at HP-HT [77]. An alternative explanation for the β' -phase at higher pressures is the presence of kinetic barriers [78]. To close this discussion we would like to emphasise the point that the PSO technique takes into account shock data as well as static data in the fitting process, and that the overall result includes a misfit with some of the experimental data [32]. The PSO calculated P - T phase boundaries, shown in grey in figure 6, are therefore generated as a balance of best fits to the available experimental data.

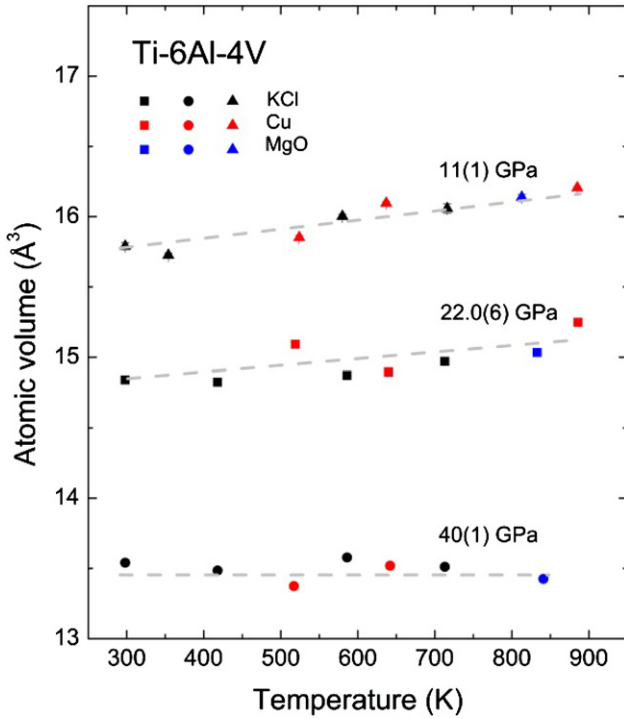


Figure 7. The variation in the atomic volume of Ti-6Al-4V as a function of temperature, at pressures 11(1), 22.0(6) and 40(1) GPa generated using KCl, Cu and MgO thermal EoSs. Ti-6Al-4V is in the α -phase at 11 and 22 GPa and in the ω -phase at 40 GPa. The uncertainties are absorbed into the data-points. The dashed grey lines have been added as a visual guide.

3.3. P - V - T EoS

Since our data were collected from three synchrotron visits, it is worth considering the impact an analysis of three separate datasets may have on the overall P - V - T EoS. Firstly, errors inadvertently introduced during the setting up of the beamlines could lead to systematic errors propagating into the data. These effects are difficult to quantify but are assumed to be negligible since detector calibrations were performed using x-ray standards (CeO_2 , LaB_6 and Si) at the start of each experiment. Secondly, the selection of a range of pressure media and markers for these experiments may give rise to dissimilar pressure environments and inconsistent pressure values. We used thermal EoSs for KCl [53], MgO [55] and Cu [56] to determine sample pressures. In figure 7, the measured atomic volumes for Ti64 are plotted against temperature, at pressures 11(1), 22.0(6) and 40(1) GPa, generated using the KCl, MgO and Cu thermal EoSs. The effects of thermal expansion on atomic volume decrease with increasing pressure. The lack of scatter in the data suggests the overall impact of the different DAC loadings on the volume analysis is not critical and therefore these variations can be discounted as limiting factors in the determination of a P - V - T EoS for Ti64.

The thermal EoS of a material can be defined as:

$$P(V, T) = P(V, T_0) + P_{\text{th}}(V, T), \quad (2)$$

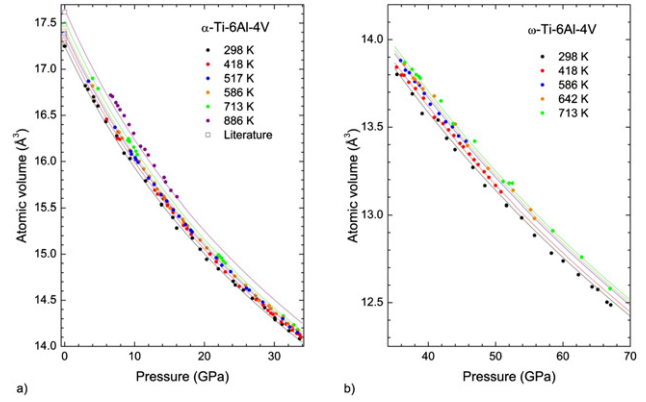


Figure 8. Pressure–volume–temperature data for (a) α -Ti-6Al-4V and (b) ω -Ti-6Al-4V. The solid lines correspond to EOS fits to the data. To ease interpretation of the data, we have omitted a number of isotherms from these figures.

where $P(V, T_0)$ represents the RT isothermal EoS component and $P_{\text{th}}(V, T)$ the thermal component. The thermal expansion of a material is given by

$$V_{0T} = V_{00} \exp \int_{T_{\text{ref}}}^T \alpha(T) dT \quad (3)$$

where T_{ref} is 298 K, V_{00} is the volume at 298 K, and $\alpha(T)$ is the coefficient of thermal expansion. The Berman model [79] can be used to describe the effects of non-linear thermal expansion on the variation of the volume with temperature, and at constant pressure:

$$V_{0T} = V_{00} \left(1 + \alpha_0 (T - T_{\text{ref}}) + \frac{1}{2} \alpha_1 (T - T_{\text{ref}})^2 \right), \quad (4)$$

where α is treated as a constant. For small changes in volume, the thermal expansion can be approximated to

$$\alpha \approx \alpha_0 + \alpha_1 (T - T_{\text{ref}}), \quad (5)$$

where α_0 is the thermal expansion coefficient at 298 K [80].

A P - V - T EoS was generated for α -Ti64 and ω -Ti64 using the least-squares fitting programme *EoSFit7* [80, 81]. Isothermal data generated at 298, 418, 517, 586, 713 and 886 K were used to generate the thermal EoS for α -Ti64, and isotherms at 298, 418, 586, 642 and 713 K were used for ω -Ti64. For both Ti64 phases, a BM3 EoS was fit to the RT data, giving the EoS parameters reported in section 3.1.

The isotherms for α -Ti64 are shown in figure 8(a) along with the best fits to the data. In figure 8(b), we show the isotherms and fits for ω -Ti64. The corresponding EoS parameters for both phases are presented in table 2 alongside previously published parameters for pure Ti at HP–HT [20]. There is good agreement with the values reported for pure Ti [20]. The negative value for $(\partial K_0 / \partial T)_P$ in Ti64 indicates a reduction in the bulk modulus with increasing temperature. Between RT and ~ 900 K, this corresponds to a decrease in the bulk modulus of $\sim 15\%$ for α -Ti64 and $\sim 6\%$ for ω -Ti64.

Table 2. P – V – T EoS parameters generated using a 3rd order Birch–Murnaghan model at RT and a Berman model for the thermal component.

	V_0 (\AA^3)	K_0 (GPa)	K'_0	α_0 (K^{-1})	α_1 (K^{-2})	$(\partial K_0/\partial T)_P$ (GPa K^{-1})
α -Ti-6Al-4V	17.25(4)	110(2)	3.8(2)	4.1(6) 10^{-5}	3(2) 10^{-8}	–0.028(3)
ω -Ti-6Al-4V	16.8(2)	115(8)	4.6(8)	3.0(9) 10^{-5}	1.0(4) 10^{-8}	–0.011(2)
α -Ti [20]	17.64(1)	114(3)	4.0 ^a	1.2(6) 10^{-5}	2.5(1.1) 10^{-8}	–0.011
ω -Ti [20]	17.29(1)	107(3)	—	6.5(3.5) 10^{-6}	2.8(6) 10^{-8}	–0.0095

^a K'_0 was fixed to derive a value for K_0 .

4. Conclusion

Commercial powdered polycrystalline Ti64 has been investigated at HP–HT using DACs and a Bridgman-type cell. ADXRD data up to 95 GPa and between RT and 886 K were collected using membrane-driven DACs. Resistivity data up to 12 GPa, and at temperatures between RT and 1500 K were collected using a Bridgman-type cell.

The data has been combined to generate for the first time a phase diagram in P – T space for Ti64. This work confirms the suppression of the $\alpha \rightarrow \omega$ transition in Ti64 up to ~ 30 GPa. For low purity Ti64 (this sample), the $\alpha \rightarrow \omega$ transition appears to be insensitive to the pressure environment in a DAC and also to temperatures between RT and ~ 900 K. On decompression, there is a pronounced hysteresis in ω -Ti64. The $\omega \rightarrow \alpha$ transition is sensitive to temperature, and transforms back into the α phase at higher pressures than is the case at lower temperatures. Our calculated solid–solid phase boundaries using the PSO method are consistent with these results and with previously published shock and static Ti64 data. Our proposed α – β – ω triple point appears to occur at the same temperature as that proposed for pure Ti, but shifted from ~ 8 GPa to ~ 30 GPa. In addition, we have derived the thermal EoSs for α -Ti64 and ω -Ti64 and found the agreement with α -Ti and ω -Ti to be good.

Data availability statement

The data that support the findings of this study are available upon reasonable request from the authors.

Acknowledgments

©British Crown Owned Copyright 2021/AWE. Published with permission of the Controller of Her Britannic Majesty's Stationary Office. DE thanks the financial support to this research provided by the Spanish Ministry of Science, Innovation and Universities, and the European Fund for Regional Development under Grant Nos. PID2019-106383GB-C41 and RED2018-102612-T (MALTA Consolider) and by Generalitat Valenciana under Grant Prometeo/2018/123 EFI-MAT. This work was performed under the auspices of the U.S. Department of Energy by Lawrence Livermore National Laboratory under Contract DE-AC52-07NA27344. MIM is grateful to AWE for the award of a William Penney Fellowship. CP acknowledges the financial support of the Spanish Ministerio de Economía y Competitividad (Mineco Project No. FIS2017-83295-P). We thank

ALBA synchrotron and Diamond Light Source for access to beamlines MSPD (Alba 2013100660) and I15 (EE8176 and EE9366). We also extend our thanks to CY Park at the Advanced Photon Source for his assistance in collecting data at 16-BMD.

ORCID iDs

S G MacLeod  <https://orcid.org/0000-0002-1055-2576>
D Errandonea  <https://orcid.org/0000-0003-0189-4221>
H Cynn  <https://orcid.org/0000-0003-4658-5764>
D Daisenberger  <https://orcid.org/0000-0001-5311-4747>
M I McMahon  <https://orcid.org/0000-0003-4343-344X>
C Popescu  <https://orcid.org/0000-0001-6613-4739>

References

- [1] Peters M, Hemptenmacher J, Kumpfert J and Leyens C 2003 *Titanium and Titanium Alloys: Fundamentals and Applications* ed C Leyens and M Peters (Weinheim: Wiley-VCH) pp 1–35
- [2] Collings E W 1984 *The Physical Metallurgy of Titanium Alloys* (Metals Park, OH: American Society for Metals)
- [3] Veiga C, Devim J P and Loureiro A J R 2012 *Rev. Adv. Mater. Sci.* **32** 133
- [4] Cezaırlıyan A, McClure J L and Taylor R 1977 *J. Res. Natl. Bur. Stand A* **81A** 251
- [5] Chesnut G N, Velisavljevic N, Sanchez L 2007 *Shock Compression of Condensed Matter* ed M Elert *et al* (New York: AIP) pp 27–30
- [6] MacLeod S G, Tegner B E, Cynn H, Evans W J, Proctor J E, McMahon M I and Ackland G J 2012 *Phys. Rev. B* **85** 224202
- [7] Velisavljevic N, MacLeod S and Cynn H 2012 *Titanium Alloys—towards Achieving Enhanced Properties for Diversified Applications* ed A K M N Amin (Croatia: IntechOpen) pp 67–86
- [8] Halevy I, Zamir G, Winterrose M, Sanjit G, Grandini C R and Moreno-Gobbi A 2010 *J. Phys.: Conf. Ser.* **215** 012013
- [9] Xia H, Duclos S J, Ruoff A L and Vohra Y K 1990 *Phys. Rev. Lett.* **64** 204
- [10] Xia H, Parthasarathy G, Luo H, Vohra Y K and Ruoff A L 1990 *Phys. Rev. B* **42** 6736
- [11] Vohra Y K, Sikka S K, Vaidya S N and Chidambaram R 1977 *J. Phys. Chem. Solids* **38** 1293
- [12] Vohra Y K 1978 *J. Nucl. Mater.* **75** 288
- [13] Vohra Y K and Spencer P T 2001 *Phys. Rev. Lett.* **86** 3068
- [14] Akahama Y, Kawamura H and Le Bihan T 2001 *Phys. Rev. Lett.* **87** 275503
- [15] Ahuja R, Dubrovinsky L, Dubrovinskaia N, Osorio Guillen J M, Mattesini M, Johansson B and Le Bihan T 2004 *Phys. Rev. B* **69** 184102
- [16] Errandonea D, Meng Y, Somayazulu M and Häusermann D 2005 *Physica B* **355** 116

- [17] Velisavljevic N, Jacobsen M K and Vohra Y K 2014 *Mater. Res. Express* **1** 035044
- [18] Errandonea D, Schwager B, Ditz R, Gessmann C, Boehler R and Ross M 2001 *Phys. Rev. B* **63** 132104
- [19] Dewaele A, Stutzmann V, Bouchet J, Bottin F and Mezouar M 2015 *Phys. Rev. B* **91** 134108
- [20] Zhang J, Zhao Y, Hixson R S, Gray G T, Wang L, Utsumi W, Hiroyuki S and Takanori H 2008 *Phys. Rev. B* **78** 054119
- [21] Zhang J, Zhao Y, Hixson R S, Gray G T, Wang L, Utsumi W, Hiroyuki S and Takanori H 2008 *J. Phys. Chem. Solids* **69** 2559
- [22] Akahama Y, Kawaguchi S, Hirao N and Ohishi Y 2020 *J. Appl. Phys.* **128** 035901
- [23] Stutzmann V, Dewaele A, Bouchet J, Bottin F and Mezouar M 2015 *Phys. Rev. B* **92** 224110
- [24] Rosenberg Z, Meybar Y and Yaziv D 1981 *J. Phys. D: Appl. Phys.* **14** 261
- [25] Morris C E, Winkler M A and Mitchell A C 1988 *Shock Waves in Condensed Matter* ed S C Schmidt and N C Holmes (Amsterdam: North-Holland) pp 155–8
- [26] Gray G T, Morris C E and Lawson A C 1993 *Proc. of Titanium '92: Science and Technology* ed F H Froes and I L Caplan (Warrendale: Minerals, Metals, and Materials Society) 225–32
- [27] Winfree N A, Chhabildas L C, Reinhart W D, Carroll D E, Kerley G I 2002 *Shock Compression of Condensed Matter* ed M D Furnish *et al* (New York: AIP) pp 75–8
- [28] Bourne N K, Millett J C F and Gray G T 2009 *J. Mater. Sci.* **44** 3319
- [29] Sollier A, Bouyer V, Maillat J-B and Voltz C 2009 *DYMAT 2009—9th Int. Conf. on the Mechanical and Physical Behaviour of Materials under Dynamic Loading* (EDP Sciences) 207–11
- [30] Ren Y, Xue Z, Luo W, Ren Y and Zhang Y 2018 *Mech. Mater.* **117** 1
- [31] Cox G A and Christie M A 2015 *J. Phys.: Condens. Matter* **27** 405201
- [32] Cox G A 2018 *Shock Compression of Condensed Matter* ed R Chau *et al* (New York: AIP) p040002
- [33] Kerley G I 2002 *Technical Report SAND2003-3785* Sandia National Laboratories, Albuquerque, New Mexico 87185, and Livermore, California 94550
- [34] Trunin R F, Simakov G V and Medvedev A B 1999 *High Temp.* **37** 851
- [35] Greeff C W, Trinkle D R and Albers R C 2001 *J. Appl. Phys.* **90** 2221
- [36] Cerreta E, Gray G T, Lawson A C, Mason T A and Morris C E 2006 *J. Appl. Phys.* **100** 013530
- [37] Jones D R, Morrow B M, Trujillo C P, Gray G T and Cerreta E K 2017 *J. Appl. Phys.* **122** 045902
- [38] Joshi K D, Jyoti G, Gupta S C and Sikka S K 2002 *Phys. Rev. B* **65** 052106
- [39] Pecker S, Eliezer S, Fisher D, Henis Z and Zinamon Z 2005 *J. Appl. Phys.* **98** 043516
- [40] Verma A K, Modak P, Rao R S, Godwal B K and Jeanloz R 2007 *Phys. Rev. B* **75** 014109
- [41] Hennig R G, Lenosky T J, Trinkle D R, Rudin S P and Wilkins J W 2008 *Phys. Rev. B* **78** 054121
- [42] Hao Y-J, Zhang L, Chen X-R, Li Y-H and He H-L 2008 *Solid State Commun.* **146** 105
- [43] Mei Z-G, Shang S, Wang Y and Liu Z-K 2009 *Phys. Rev. B* **79** 134102
- [44] Mei Z-G, Shang S-L, Wang Y and Liu Z-K 2009 *Phys. Rev. B* **80** 104116
- [45] Hu C-E, Zeng Z-Y, Zhang L, Chen X-R, Cai L-C and Alfè D 2010 *J. Appl. Phys.* **107** 093509
- [46] Argaman U, Eidelstein E, Levy O and Makov G 2015 *Mater. Res. Express* **2** 016505
- [47] Trinkle D R, Hennig R G, Srinivasan S G, Hatch D M, Jones M D, Stokes H T, Albers R C and Wilkins J W 2003 *Phys. Rev. Lett.* **91** 025701
- [48] Gao L, Ding X, Lookman T, Sun J and Salje E K H 2016 *Appl. Phys. Lett.* **109** 031912
- [49] Hennig R G, Trinkle D R, Bouchet J, Srinivasan S G, Albers R C and Wilkins J W 2005 *Nat. Mater.* **4** 129
- [50] Trinkle D R, Hatch D M, Stokes H T, Hennig R G and Albers R C 2005 *Phys. Rev. B* **72** 014105
- [51] Zarkevich N A and Johnson D D 2016 *Phys. Rev. B* **93** 020104
- [52] Goodfellow Cambridge Ltd 2012 private communication.
- [53] Tateno S, Komabayashi T, Hirose K, Hirao N and Ohishi Y 2019 *Am. Mineral.* **104** 718
- [54] Dorogokupets P I and Dewaele A 2007 *High Press. Res.* **27** 431
- [55] Speziale S, Zha C-S, Duffy T S, Hemley R J and Mao H-k. 2001 *J. Geophys. Res.* **106** 515
- [56] Cynn H *et al* 2012 *APS March Meeting* (Boston, MA)(Feb 27–Mar 02)
- [57] Jenei Z, Cynn H, Visbeck K and Evans W J 2013 *Rev. Sci. Instrum.* **84** 095114
- [58] Stinton G W, MacLeod S G, Cynn H, Errandonea D, Evans W J, Proctor J E, Meng Y and McMahon M I 2014 *Phys. Rev. B* **90** 134105
- [59] Cazorla C, MacLeod S G, Errandonea D, Munro K A, McMahon M I and Popescu C 2016 *J. Phys.: Condens. Matter* **28** 445401
- [60] Errandonea D, MacLeod S G, Ruiz-Fuertes J, Burakovsky L, McMahon M I, Wilson C W, Ibañez J, Daisenberger D and Popescu C 2018 *J. Phys.: Condens. Matter* **30** 295402
- [61] Fauth F, Peral I, Popescu C and Knapp M 2013 *Powder Diffr.* **28** S360
- [62] Hammersley A P, Svensson S O, Hanfland M, Fitch A N and Häusermann D 1996 *High Press. Res.* **14** 235
- [63] Prescher C and Prakapenka V B 2015 *High Press. Res.* **35** 223
- [64] Larson A C and von Dreele R B 2004 *LANL Report 86-748* Los Alamos National Laboratory
- [65] JADE 9.4.5 software 2012 (Livermore, CA-94550, USA: MDI).
- [66] Holland T J B and Redfern S A T 1997 *Mineral. Mag.* **61** 65
- [67] Errandonea D, Segura A, Sánchez-Royo J F, Mun-|Atoz V, Grima P, Chevy A and Ulrich C 1997 *Phys. Rev. B* **55** 16217
- [68] Bean V E, Akimoto S, Bell P M, Block S, Holzäpfel W B, Manghnani M H, Nicol M F and Stishov S M 2006 *Physica B+C* **139** 52
- [69] Errandonea D, Martínez-García D, Segura A, Ruiz-Fuertes J, Lacomba-Perales R, Fages V, Chevy A, Roa L and Muñoz-San José V 2006 *High Press. Res.* **26** 513
- [70] Errandonea D 2010 *J. Appl. Phys.* **108** 033517
- [71] Birch F 1952 *J. Geophys. Res.* **57** 227
- [72] Vinet P, Ferrante J, Rose J H and Smith J R 1987 *J. Geophys. Res.* **92** 9319
- [73] Balog P S and Secco R A 1999 *J. Phys.: Condens. Matter* **11** 1273
- [74] Alchagirov A B, Perdew J P, Boettger J C, Albers R C and Fiolhais C 2001 *Phys. Rev. B* **63** 224115
- [75] Mehta S 2006 *Shock Compression of Condensed Matter* ed M D Furnish *et al* (New York: AIP) pp 258–61
- [76] Johnson J N, Hayes D B and Asay J R 1974 *J. Phys. Chem. Solids* **35** 501
- [77] Anzellini S *et al* 2018 *Phys. Rev. Mater.* **2** 083608
- [78] Errandonea D *et al* 2020 *Commun. Mater* **1** 60
- [79] Berman R G 1988 *J. Petrol.* **29** 445
- [80] Angel R J, Gonzalez-Platas J and Alvaro M 2014 *Z. Kristallogr.* **229** 405
- [81] Gonzalez-Platas J, Alvaro M, Nestola F and Angel R 2016 *J. Appl. Crystallogr.* **49** 1377